

# Detecting Polar Stratospheric Clouds With Zenith-Looking Photometers

C.-F. Enell<sup>1</sup>, K. Stebel<sup>1</sup>, T. Wagner<sup>2</sup>, U. Frieb<sup>2</sup>, K. Pfeilsticker<sup>2</sup>, and U. Platt<sup>2</sup>

<sup>1</sup>Swedish Institute of Space Physics, Kiruna, Sweden

<sup>2</sup>Institute of Environmental Physics, Heidelberg University, Germany

Received: 26.11.2001 – Accepted: 14.6.2002

**Abstract.** It has been suggested to use the zenith-sky colour index (CI) as a means of obtaining an indication of the presence of polar stratospheric clouds (PSCs). This article discusses the use of the CI method for statistical purposes. Comparing CI data from a UV/visible spectrometer system (located at Kiruna, Sweden) with assimilated synoptic-scale temperature data, we conclude that the CI method yields a lower limit of PSC presence during sunrise and sunset. It is likely that tropospheric cloud presence at the tangent point of zenith-scattered solar rays is one reason for this discrepancy.

## 1 Introduction

Polar stratospheric clouds (Størmer, 1930; Hoesstvedt, 1960; Poole et al., 1988), commonly abbreviated PSCs, develop in the cold winter polar vortex. In the Arctic this is often a result of local cooling in mountain-induced waves (see e.g. Dörnbrack et al., 2000, and references therein). Both the large-scale temperature fields and the local wave activity have a large interannual variability. This also holds true for PSC presence because of the strong temperature dependence of the involved condensation and freezing processes (Hanson and Mauersberger, 1988). It is now generally accepted that the presence of PSCs is of major importance for stratospheric chemistry, since reactions on PSC particles release active halogen species, as was recognised by Crutzen and Arnold (1986). The removal of PSC particles by sedimentation also denitrifies the polar stratosphere, which further enhances ozone depletion. See e.g. Gao et al. (2001) for recent observations of denitrification in the Arctic.

Since the wavelength dependence of the scattering cross sections of typical aerosols is a function of the Mie (Bohren and Huffman, 1983) size parameter  $x = 2\pi r/\lambda$ , rather than a quantity of  $O(\lambda^{-4})$  as for molecular dipole scattering, an aerosol layer above the site of measurement will cause a redshift of the zenith-sky spectral radiance during twilight

(Rozenberg, 1966). This is used in the context of PSC detection by Sarkissian et al. (1991, 1994, 1998); Enell et al. (1999) and in the present work.

## 2 Data analysis

A UV/visible spectrometer system has been in operation in Kiruna since December 1996. The system records spectra continuously during daylight and twilight. Its primary purpose is the retrieval of column densities of BrO (Sinnhuber et al., 2002), OCIO, ozone and NO<sub>2</sub> by means of Differential Optical Absorption Spectroscopy (DOAS) analysis (Platt, 1994) in selected wavelength windows. In DOAS only absorption cross sections varying rapidly with respect to the wavelength range are considered and the broad-band spectral distribution is disregarded. The latter, however, is determined by aerosol scattering as well as the spectral sensitivity of the instrument, etc.

The simplest measure of changes due to varying broad-band scattering phenomena is the colour index

$$CI(SZA) = \frac{I(\lambda_1, SZA)}{I(\lambda_2, SZA)}$$

where  $I(\lambda_1, SZA)$  and  $I(\lambda_2, SZA)$  are the integrated spectral counts at the solar zenith angle SZA in wavelength intervals at the ends of the spectral interval covered by the detector. These should preferably be chosen outside rapidly varying absorption bands, or varying trace gas concentrations along the optical path (Hulburt, 1953) will affect the colour index. Choosing  $\lambda_1 > \lambda_2$ , a redshift of the spectral radiance will correspond to a colour index increase. Since the colour index is a relative quantity, no absolute calibration of the detector is needed. The required processing of the spectra is subtraction of the offset voltages and dark currents of the detector photodiodes, and wavelength calibration. Detector offset and dark current are recorded every night and subtracted from the raw data. An accurate wavelength calibration for each spectrum is obtained from the positions of

Correspondence to: C.-F. Enell

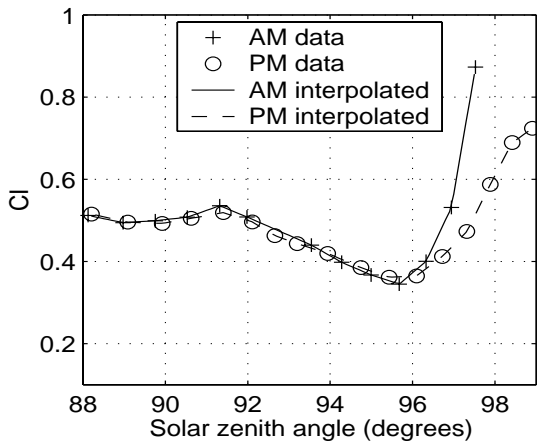


**Fig. 1.** CI development during sunrise (AM) and sunset (PM) on April 18, 2001, a clear day without PSCs. The AM and PM curves follow each other due to the absence of clouds.

the solar Fraunhofer lines (Ingelstam et al., 1988). This is a minor correction; Hg and Ne lamp spectra indicate that the spectrometer has been stable to within one channel between calibrations.

All results below have been retrieved using wavelength intervals of  $\pm 2$  nm around 680 nm ( $\lambda_1$ ) and 385 nm ( $\lambda_2$ ). The reason for this choice is that these wavelengths are at the ends of the interval covered by the spectrometer and outside ozone absorption bands. Nominal integration times during twilight are 5 minutes for  $90^\circ < \text{SZA} < 93^\circ$  and 10 minutes for  $\text{SZA} > 93^\circ$ . The instrument adjusts these integration times automatically to reach a detector saturation of 60–90%. The solar zenith angle SZA is calculated at the average time of spectral integration.

### 3 CI observations

The development of CI during sunrise (AM) and sunset (PM) on a clear day without PSCs (April 18, 2001) is shown in Figure 1. A decrease of the clear-sky CI (blueshift) after sunset, due to multiple scattering (Ougolnikov, 1999, and private communication) and possibly extinction by ozone and aerosols, can be seen in the interval  $91^\circ < \text{SZA} < 96^\circ$ . Figure 2 shows an example of the twilight CI development on January 25, 2000, when clearly visible PSCs (mother-of-pearl clouds) were observed over Kiruna. Our data series suggests that the most significant signature of PSC presence is a peak (significant redshift) close to  $\text{SZA} = 94^\circ$ , which is consistent with an altitude of maximal scattering probability (Solomon et al., 1987) above 20 km, i.e. typical PSC altitudes. Another feature apparent in Figure 2 is a CI increase at high solar zenith angles (above  $96^\circ$ ) which can sometimes be observed due to detector noise or local light sources dominating over the zenith-scattered solar light. In the raw spectra of these occasions the 546 nm green Hg line is generally a dominant feature. This is, however, no serious limitation to PSC detectability, since there is little or no single-scattering

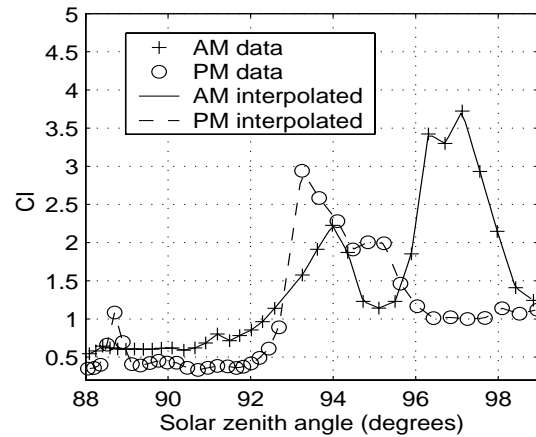


**Fig. 2.** CI peaks on January 25, 2000, a day with PSCs over Kiruna. The peaks around 94 degrees are due to the presence of PSCs. The peak at a SZA of 97 degrees is very likely due to local light sources; the contribution from single zenith scattering is negligible at this SZA. Note that the CI scale is  $5\times$  that of Figure 1.

contribution to the zenith radiance from PSC altitudes (See Table 1) at these SZAs.

## 4 PSC detectability

### 4.1 PSC detection thresholds

Because of the rapidly changing solar zenith angle during twilight and the long integration times, there are typically few data points in the interval around 94 degrees. The colour index variation often also shows a large fluctuating component due to changing cloudiness (see Section 4.2), precipitation, local light sources, etc. Here we examine three different indicators of PSC-induced redshift of the zenith sky:

(A) the absolute value of the CI interpolated at  $\text{SZA} = 94^\circ$ , (B) the normalised colour index (Sarkissian et al., 1991; Enell et al., 1999), i.e. the ratio of the colour index to its value at sunrise/sunset ( $\text{SZA} = 90^\circ$ ), and (C), identification of peaks around  $\text{SZA} = 94^\circ$  by a polynomial fit. The parabola

$$P(X) = CI(94^\circ) - AX, X = (\text{SZA} - 94)^\circ$$

fits the data best in the least-squares sense when

$$A = \frac{CI(94^\circ) \sum_n X_n - \sum_n CI_n X_n}{\sum_n X_n^2}$$

where the summations are over the available data points during twilight.

These three CI measures have been calculated for data from January–March and November–December of 1997, 1998 and 1999 and January–March 2000. (As in Enell et al. (1999), it must be remarked that there are data gaps during the coldest winter weeks, coincident with the Christmas holidays when instrument maintenance is sparse.) In Figure 3 the results are compared with the assimilated synoptic temperatures obtained from the European Centre for Medium-Range Weather

Forecasts (ECMWF). The different CI measures are plotted versus the coldest temperature with respect to the condensation temperature of nitric acid trihydrate ( $T_{NAT}$ ) occurring on the levels 400K, 475K, 550K and 675K above Kiruna in the  $2.5^\circ \times 2.5^\circ$  ECMWF grid.  $T_{NAT}$  was calculated for each level according to Hanson and Mauersberger (1988), with 4.6 ppm  $H_2O$  and a  $HNO_3$  profile from the Limb IR Monitor of the Stratosphere (LIMS).

The largest number of significant CI reddenings are obtained at low synoptic temperatures. The highest values are from January 1997, when a visible layer of mother-of-pearl clouds persisted for several days. A high value at  $T - T_{NAT} \approx 8$  is present in the absolute and normalised colour index series but absent in the polynomial fit. This point was found to be the result of the entrance lenses accidentally being covered after a system restart. A basic requirement on all detection methods is the capability to filter out such outlier values. The peak coefficient  $A$  can be thought of as a filtered index calculated from all available data points in the twilight SZA interval. Due to this filtering,  $A$  is large only for  $T < T_{NAT}$ . We therefore consider the peak fit to provide the best threshold condition out of these methods. Sarkissian et al. (1991) argued that normalisation of the CI to unity at SZA =  $90^\circ$  would correct for effects unrelated to stratospheric scattering. A comparison (Fig. 4) between the three indices for the entire available dataset (winter months from December 1996 until March 2002) shows that the opposite effect can occur. Division by a value (CI at SZA =  $90^\circ$ ) which has a large contribution from direct tropospheric scattering, or even has to be extrapolated during the polar winter when the sun is below the horizon, introduces unnecessary noise. The absolute value of the CI shows less scatter than the normalised CI, which is sometimes even negative due to the extrapolation error.

A striking result is that a large number of low CI values are obtained at all synoptic temperatures. PSC observations at temperatures above synoptic  $T_{NAT}$  could be expected since local temperatures are affected by mountain wave induced cooling. This even includes non-equilibrium effects, causing unexpected presence of liquid or solid PSCs (Voigt et al., 2000; Tsias et al., 1997). The result may indicate that detectable PSCs develop only as a consequence of supercooling below  $T_{NAT}$ . The possibility that the abscissae of Figure 3 should be shifted up to 5K due to systematic biases in the meteorological model is also non-negligible (Manney et al., 2001). Calibration against other observations and further radiative transfer modelling is required to determine the sensitivity. However, because of the observational geometry, the interpretation that the PSC presence is underestimated is also plausible.

#### 4.2 Geometrical and meteorological constraints

As demonstrated e.g. by Ougolnikov (1999), a major contribution to the brightness of the twilight sky emanates from multiple scattering. However, enhanced scattering by PSCs will occur as single-volume scattering within the field of view

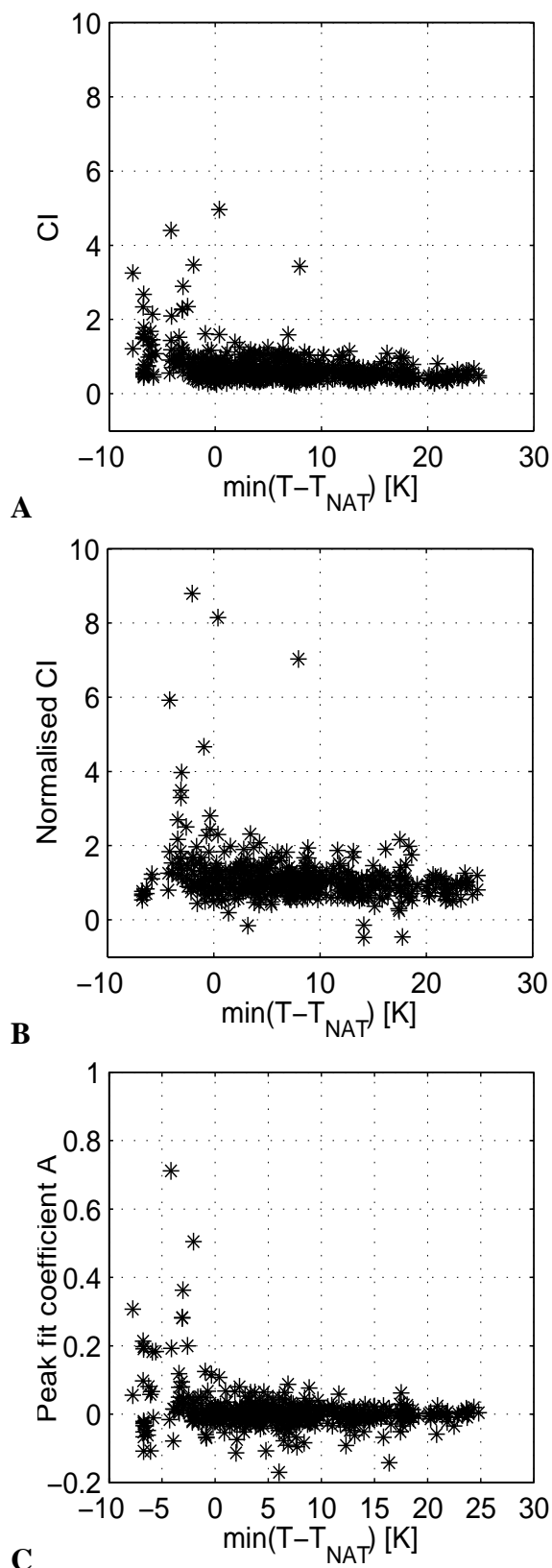


**Fig. 3.** Scatter plots of colour indices vs. the minimum of  $T - T_{NAT}$  on any of the ECMWF levels 400K, 475K, 550K and 675K. A: Absolute value of CI at SZA =  $94^\circ$ . B: Normalised CI. Unphysical values close to zero have been removed. Negative values are kept to show the influence of interpolation errors. C: Polynomial coefficient  $A$ .

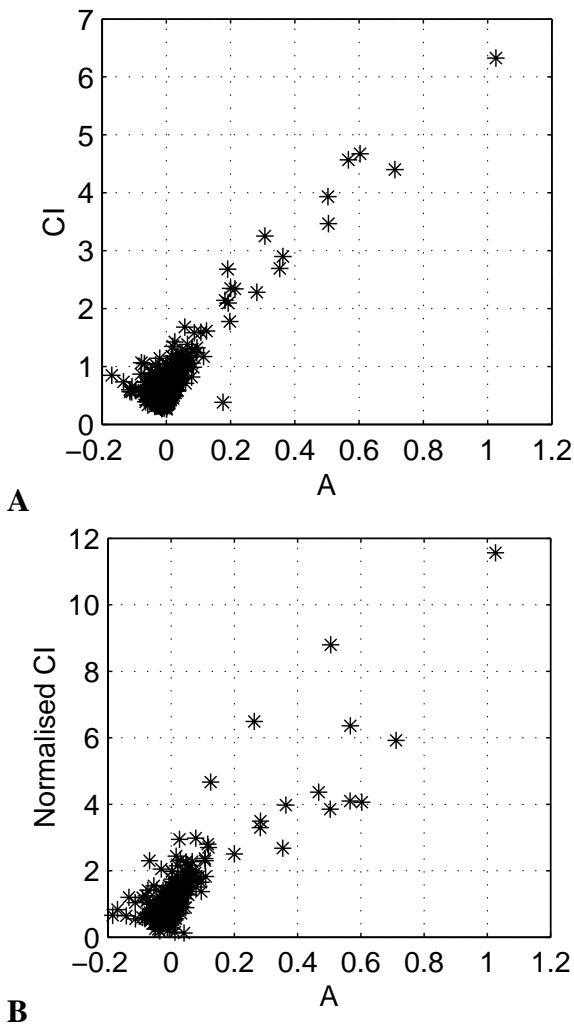


**Fig. 4.** Two CI measures vs.  $A$ , the peak fit coefficient. **A:** the absolute value at  $SZA = 94^\circ$ . **B:** Normalised CI. These plots include the entire time series from December 1996 until March 2002.

of the instrument. Therefore, the single-scattering geometry shown in Figure 5 is important. The tangent height  $H_T$  of solar rays reaching the PSC (Table 1) is an important parameter to consider (Meinel and Meinel, 1983). As stated above, the sun is below the horizon even at typical PSC heights for solar zenith angles exceeding 95 degrees.

$H_o$	$H_{to}(92^\circ)$	$H_{to}(93^\circ)$	$H_{to}(94^\circ)$	$H_{to}(95^\circ)$
18	14.1	9.2	2.4	–
20	16.1	11.2	4.4	–
22	18.1	13.2	6.4	–
24	20.1	15.2	8.4	–
26	22.1	17.2	10.4	1.6
28	24.1	19.2	12.4	3.6

**Table 1.** Tangent heights [km] corresponding to PSC heights between 18 and 30 km at solar zenith angles between 92 and 95 degrees. A spherical Earth with a radius of 6378 km has been assumed and atmospheric refraction has been ignored.

The radiosonde average winter tropopause height at Kiruna is  $9.5 \pm 1.8$  kilometres. Thus a varying cloud cover can exist

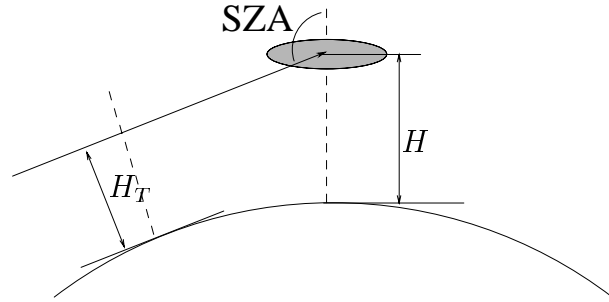


**Fig. 5.** The geometry of zenith scattering in the single-scattering approximation.  $SZA$  is the solar zenith angle,  $H$  the mean altitude of an object (PSC layer etc), and  $H_T$  the corresponding tangent height.

everywhere below that altitude, which implies that the contribution to zenith-scattering by all PSCs at altitudes below approximately 27 kilometres will be modified by tropospheric clouds in the vicinity of the tangent point (the difference between sunsets with clear and cloudy weather at the tangent point is also visually apparent). The effect of PSCs can therefore be screened out, depending on the character of tropospheric cloudiness. Normalisation of the CI clearly does not compensate for this effect, since single PSC scattering at  $SZA = 90^\circ$  is not influenced by the troposphere.

Moreover, during the PSC season the solar azimuth at the relevant zenith angles varies from close to the south in mid-winter to the east/west in March, which may even cause a seasonal variation in PSC detectability since the tropospheric climate (and hence cloud cover) is highly locally varying in the proximity of the Scandinavian mountain range.

## 5 Summary

It has been demonstrated that the zenith-sky colour index (CI) can be used as a means for passive optical detection of stratospheric clouds. Three different definitions of PSC indication CI thresholds have been examined. A least-squares fit of polynomials to CI peaks during twilight provides a useful threshold condition. Large values of the PSC index are obtained at temperatures below  $T_{NAT}$ . We suggest, however, that as a quantitative means of obtaining PSC statistics it very likely yields a lower limit. The importance of this underestimation remains to be quantified experimentally, e.g. by correlation with co-located lidar, photographic, visual and satellite observations, and theoretically by radiative transfer modelling.

The present principal application of the method still applies, namely the qualitative indication of PSC presence in cases when local tropospheric conditions prevent direct PSC observations. This has proven to be of practical use, not least when planning balloon launches of in-situ PSC experiments.

*Acknowledgements.* We want to thank Dr. K-H Fricke for pointing out the presence of curves with peaks at high solar zenith angles, which turned out to be the result of local light pollution.

## References

- Bohren, C. F. and Huffman, D. R., *Absorption and scattering of light by small particles*, John Wiley and Sons, Inc., 1983.
- Crutzen, P. J. and Arnold, F., Nitric acid cloud formation in the cold Antarctic stratosphere: a major cause for the springtime "ozone hole", *Nature*, 324, 651–655, 1986.
- Dörnbrack, A., Leutbecher, M., Reichardt, J., A. Behrendt, K.-P. Müller, and G. Baumgarten, Relevance of mountain waves for the formation of polar stratospheric clouds over Scandinavia: Mesoscale dynamics and observations for January 1997, *J. Geophys. Res.*, 2000.
- Enell, C.-F., Steen, Å., Wagner, T., Frieß, U., and Platt, U., Occurrence of polar stratospheric clouds at Kiruna, *Ann. Geophys.*, 17, 1457–1462, 1999.
- Gao, R., Richard, E., Popp, P., Toon, G., Hurst, D., Newman, P., Holecek, J., Northway, M. W., Fahey, D., Danilin, M., Sen, B., Aikin, K., Romashkin, P., Schauffler, S., Greenblatt, J., McElroy, C., Lait, L., Bui, T., and Baumgardner, D., Observational evidence for the role of denitrification in Arctic stratospheric ozone loss, *Geophys. Res. Lett.*, 28, 2879–2882, 2001.
- Hanson, D. and Mauersberger, K., Laboratory studies of the nitric acid trihydrate: Implications for the south polar stratosphere, *Geophys. Res. Lett.*, 15, 855–858, 1988.
- Hesstvedt, E., On the physics of mother of pearl clouds, *Geofysiske Publikasjoner*, 21, 1960.
- Hulburt, E., Explanation of the brightness and color of the sky, particularly the twilight sky, *J. Opt. Soc. Am.*, 43, 113–118, 1953.
- Ingelstam, E., Rönngren, R., and Sjöberg, S., *TEFYMA, Handbok för teknisk fysik, fysik och matematik*, Sjöbergs Bokförlag AB, 1988.
- Manney, G. L., Sabutis, J. L., Pawson, S., Santee, M. L., Naujokat, B., Swinbank, R., Melvyn E. G., and Ebisuzaki, W., Lower stratospheric temperature differences between meteorological analyses in two Arctic winters and their impact on polar processing studies, *J. Geophys. Res.*, 2001.
- Meinel, A. and Meinel, M., *Sunsets, twilights, and evening skies*, Cambridge University Press, 1983.
- Ougolnikov, O. S., Twilight sky photometry and polarimetry: The problem of multiple scattering at the twilight time, *Cosm. Res. (translated from Russian)*, 37, 159–166, 1999.
- Platt, U., Differential optical absorption spectroscopy, *Air Monitoring by Spectroscopic Techniques, chapter 2*, John Wiley & Sons, Inc., 1994.
- Poole, L., Osborn, M., and Hunt, W., Lidar observations of Arctic polar stratospheric clouds 1988: Signature of small, solid particles above the frost point, *Geophys. Res. Lett.*, 15, 867–870, 1988.
- Rozenberg, G. V., *Twilight*, Plenum Press, 1966.
- Sarkissian, A., Pommereau, J.-P., and Goutail, F., Identification of polar stratospheric clouds from the ground by visible spectrometry, *Geophys. Res. Lett.*, 18, 779–782, 1991.
- Sarkissian, A., Pommereau, J., Goutail, F., and Kyrö, E., PSC and volcanic aerosol observations during EASOE by UV-visible ground-based spectrometry, *Geophys. Res. Lett.*, 21, 1319–1322, 1994.
- Sarkissian, A., Fierli, F., Goutail, F., Pommereau, J.-P., Kyrö, E., and Rummukainen, M., Frequency of occurrence of PSC above Northern Scandinavia from 1990 to 1997 from SAOZ zenith sky colour index, in *Polar stratospheric ozone 1997, Proceedings of the fourth European symposium*, edited by N. Harris, I. Kilbane-Dawe, and G. Amanatidis, vol. Air pollution research report 66, European Commission, 1998.
- Sinhaber, B.-M., Arlander, D. W., Bovensmann, H., Burrows, J. P., Chipperfield, M. P., Enell, C.-F., Frieß, U., Hendrick, F., Johnston, P. V., Jones, R. L., Kreher, K., Mohamed-Tahrin, N., Müller, R., Pfeilsticker, K., Platt, U., Pommereau, J.-P., Pundt, I., Richter, A., South, A. M., Tørnkvist, K. K., van Roozendaal, M., Wagner, T., and Wittrock, F., The global distribution of stratospheric bromine monoxide: Intercomparison of measured and modeled slant column densities, *J. Geophys. Res.*, accepted, 2002.
- Solomon, S., Schmeltekopf, A. L., and Sanders, R. W., On the interpretation of zenith sky absorption measurements, *J. Geophys. Res.*, 7, 8311–8319, 1987.
- Størmer, C., Photogrammetrische Bestimmung der Höhe von irisierenden Wolken, *Geofysiske Publikasjoner*, 5, 1930.
- Tsias, A., Prenni, A. J., Carslaw, K. S., Onasch, T. P., Luo, B. P., Tolbert, M. A., and Peter, T., Freezing of polar stratospheric clouds in orographically induced strong warming events, *Geophys. Res. Lett.*, 24, 2303–2306, 1997.
- Voigt, C., Tsias, A., Dörnbrack, A., Meilinger, S., Luo, B., Schreiner, J., Larsen, N., Mauersberger, K., and Peter, T., Non-equilibrium compositions of liquid polar stratospheric clouds in gravity waves, *Geophys. Res. Lett.*, 27, 3873–3876, 2000.